Polyelectrolyte-Coated Nanosphere Lithographic Patterning of Surfaces: Fabrication and Characterization of Electropolymerized Thin Polyaniline Honeycomb Films

Shubo Han,† Alejandro L. Briseno,† Xiangyang Shi, Daisy A. Mah, and Feimeng Zhou*

Department of Chemistry and Biochemistry, California State University—Los Angeles, Los Angeles, California 90032

Received: April 1, 2002

Well-ordered 2-D polyaniline (PAni) honeycomb films were produced by electropolymerization of aniline within the interstitial voids in assemblies of polystyrene (PS) nanospheres precoated with poly(diallyldimethylammonium chloride) and poly(sodium 4-styrenesulfonate) (PDADMAC/PSS) thin shells, followed by the extraction of the PS cores with toluene. Depositing polyelectrolyte (PE) layers onto the PS particles was found to greatly improve the uniformity of the PAni attachment onto the PS particle surface. Through a systematic variation of the PE layer number and the electropolymerization parameters, PAni honeycomb films with desirable pore sizes, pore wall widths, and film thicknesses can be fabricated. Atomic force microscopy (AFM) and scanning electron microscopy were used to study the surface features of the resulting PAni honeycomb films, whereas electrochemical quartz crystal microbalance (EQCM) and reflectance FTIR measurements were carried out to verify the redox states of the PAni films and the composite nature of the pore walls. Assemblies constituting PS particles coated with four alternating PDADMAC and PSS layers yielded densely deposited PAni honeycomb films with evenly distributed pores. The PE shells within the pores of the honeycomb structure were found not to affect the overall properties of the PAni honeycomb films (e.g., conductivity, redox properties, and ion mobility within the films). Interestingly, the presence of PE/PAni composites at the pore walls appears to enhance the rigidity of the PAni film, as the extent of pore shrinkage was observed to be smaller with films produced with the template of PS particles precoated with a four or six PE layers. PE-coated nanosphere lithography followed by electropolymerization provides a unique method for constructing honeycomb films with patterns that are tunable and pores that are modifiable.

1. Introduction

Recently, template-directed synthesis of patterned thin polymer films of micrometer and submicrometer dimensions has generated a great deal of interest.[1−12] Such immense interest stems from the exploration of the new materials for applications as diverse as porous electrodes, photonic band crystals, separation media, catalysts, and sensors.[1,13−19] Some of the templates include, but are not limited to, arrays of inorganic[2,20,21] and polymeric nanoparticles[1,3−11] and membranes containing nanometer-sized pores.[12,22,23] The template is typically used as a support for the polymer deposition and can be either part of the final composite material or removed by solvent extraction. Several reports have shown that macroporous or 3-D conductive polymers such as polypyrrole (PPy),[7,9,24] polyaniline (PAni),[8,24] and polybithiophene[24] can be formed with the colloidal particle arrays as the templates. In addition to the versatility associated with the template-directed synthesis, precise control of the surface morphology and a flexible tailoring of the pore sizes and densities can also be accomplished.

Despite the fact that a number of macroporous structures containing polymers have been reported,[1−10,25] few systematic efforts have been made to correlate the amount of conductive polymer deposition to the geometric parameters of the colloidal particle arrays. Moreover, whereas it is known that deposition of polymers onto colloidal particles is dependent on the surface parameters of the colloidal particles (e.g., size of and charges and functional groups on the colloidal particles[20,21,26−28]), attaching conductive polymers onto colloidal particles modified with a large number of charged species has not been explored. Thus, it is imperative to examine the factors affecting polymer deposition onto and into the templates to improve the properties of the final materials. Our present work is concerned with the controllable electrochemical deposition of PAni into the interstitial voids present in a highly ordered 2-D array of polyelectrolyte (PE)-coated polystyrene (PS) nanospheres. We aim to develop a methodology that will ultimately enable us to compare the experimentally measured PAni growth to the PAni deposition allowed by the free volume existing at the patterned surface. In doing so, preparative parameters can be systematically examined to improve and fine-tune the properties of the final PAni thin films.

In choosing the above system, we undertake the following approaches to ensure controllability in growing patterned conductive polymer thin films, accuracy in measuring the film growth, and validity in comparing the experimental values to those predicted by the geometric volumes in the template. First, in keeping with the consideration of controlled and predictable PAni growth, we chose electrochemical polymerization over the chemical route because of the advantages inherent to the former method (e.g., simplicity in the procedure and flexibility in altering the polymer growth rate and the amount of deposition). In addition, other in situ methods can be carried out simultaneously with the electropolymerization step (e.g., spectroelec-

* To whom correspondence should be addressed. E-mail: fzhou@calstatela.edu. Tel: (323) 343-2390. Fax: (323) 343-6490.

† These authors contributed equally to this work.

10.1021/jp0258762 CCC: $22.00
Published on Web 06/04/2002

trochemistry[29] and electrochemical quartz crystal microbalance, EQCM[30,31]), affording the possibility of accurately quantifying the amount of deposit. Second, nanosphere lithography (NSL) has been demonstrated by several research groups to be a simple, reproducible, and versatile technique for fabricating well-ordered 2-D nanoparticle and metal arrays.[32−38] A periodic 2-D array of colloidal particles has been shown by Van Duyne and co-workers to be better ordered and more defect-free than the 3-D multilayered particle network,[35−37,39] thereby making the structural parameters derived from surface characterization (e.g., atomic force microscopy (AFM) and scanning electron microscopy (SEM)) more comparable to those predicted by the geometric volumes of the pattern. The adoption of a 2-D array, instead of a 3-D network, also greatly simplifies the calculation of the total amount of PAni that can be deposited into the available interstitial spaces. Because the upper layers of colloidal particles in a 3-D network (or macroporous structures) may impose a possible hindrance to the aniline monomer diffusion from the solution to the underlying electrode surface, the use of a 2-D array should allow a better patterned PAni film to be formed. All of these factors facilitate a meaningful comparison between the PAni deposition determined experimentally (e.g., by EQCM) and the theoretical projection. Finally, we decided to predeposit the PS particles with alternating layers of polyelectrolytes and to apply them to the NSL procedure. The motivation behind this modification is driven by the well-known fact that charges on the colloidal particles (e.g., carboxylate groups on the polystyrene nanospheres) facilitate the formation of a smooth PPy film or shell.[26] However, it has been reported by Armes and co-workers and Stejeskal et al. that, perhaps because of the insufficient number of charges on the unmodified PS particle surfaces, formation of a uniform PAni coating is difficult.[40−42] Therefore, to improve the homogeneity of the PAni film, a greater number of charges should be rendered to and a somewhat hydrophobic environment should be created at the particle surface. The latter factor is known to be a kinetically preferred condition for conductive polymer growth.[43−45]

We envision that coating the PS nanospheres with PE layers via the layer-by-layer (LBL) procedure[46] might fulfill these criteria. With LBL deposition of alternatively charged PE layers, a myriad of charges can be evenly distributed onto the nanosphere surface. If a negatively charged PE layer is left as the outermost layer, the positively charged aniline monomers could be uniformly attracted to the negatively charged PE shell surface and could subsequently polymerize to PAni. Moreover, it is generally believed that the interior of the mulitlayered PE layers is relative hydrophobic.[47] Consequently, the PE thin shells can provide an ideal milieu for the uniform growth of PAni (which is hydrophobic) and the extension of PAni growth into the PE shell.

We have recently demonstrated the feasibility of forming a 2-D array of hexagonally close-packed PE-coated colloidal particles. Some of our prior knowledge concerning the template formation, the interaction of the precursor with the PE layer, and the extraction of the PS core can help us understand the present system. Because of the PE coating, the extraction of the PS inner cores upon PAni film deposition in the interstitial spaces might leave a PE shell surrounding the pores in the final PAni honeycomb film. Therefore, it is of interest to know whether the newly created PAni honeycomb film possesses properties that differ from those of a conventional PAni thin film. We show in this work that the inner walls of the uniformly distributed pores present in the PAni thin films can be modified with a desirable number of PE layers without significantly changing the important physical properties of the honeycomb films (e.g., conductivity and ion mobility within the film). Modifying the pores with PE layers, however, helps improve certain features of the PAni honeycomb structure (rigidity of thin walls around the pores) and may provide a unique means for device fabrication and sensor development.

2. Experimental Section

2.1. Materials. Aniline (Baker Chemical Co.) was doubly distilled under vacuum prior to use. $HClO_4$, NaOH, NaCl, poly(sodium 4-styrenesulfonate) (PSS, average M_w = ca. 70 000), poly(diallyldimethylammonium chloride) (PDADMAC, M_w = ca. 200 000), and toluene were all acquired from Aldrich Chemicals (Milwaukee, WI). The PS nanospheres with a diameter of 600 nm were obtained from Interfacial Dynamics Inc. (Portland, OR) as a 0.8 wt % solution in water. All of the solutions were prepared with water purified by a Millipore Milli-Q Plus 185 purification system.

2.2. Electrodes. The use of 9.995-MHz gold-coated crystals for EQCM studies has been described elsewhere.[48−50] Thin gold film substrates for self-assembling PE-coated particles were prepared by sputtering 60 nm of gold with a 0.5-nm-thick underlayer of chromium onto thin glass slides (Fisher Scientific) using a Kurt J. Lesker device (model 108; Clairton, PA). Both the QCM crystals and the gold slides were cleaned with a piranha solution and rinsed with water. *CAUTION: Piranha solution reacts violently with organic solvents and is a skin irritant. Extreme caution should be exercised when handling piranha solution*. The area of the gold film disk was 0.212 cm^2 (QCM active area), and the portion of the stem of the keyhole that was exposed to solutions constituted another 0.048 cm^2 (total conductive area = 0.26 cm^2).

2.3. Instrumentation. A CHI 411 electrochemical quartz crystal microbalance (CH Instruments; Austin, TX) was used to monitor the electropolymerization and the ion transport processes within the PAni honeycomb films. Reflectance FTIR measurements were conducted with an Equinox 55 FTIR (Bruker Optics Inc., Billerica, MA) housing a variable-angle specular reflectance accessory (VeeMax II, Pike Instruments, Madison, WI). An average of 32 scans were performed to produce each spectrum. AFM measurements were conducted by using an AFM equipped with a magnetic alternating current (MAC) mode (Molecular Imaging, Phoenix, AZ). Both contact and MAC modes were employed for the characterization of the PAni honeycomb film surfaces. The amplitude change of the probe was sufficiently low; consequently, the imaging was nondestructive to the samples.[50] SEM measurements were carried out with a Cambridge Stereoscan 250 instrument operated at 20 kV.

For the conductivity measurement, a PAni honeycomb film was grown across a 11-μm gap between two 1.8-cm-wide and 20-nm-thick Au stripes deposited onto a glass slide. The resistance of the PAni film was measured using a digital multimeter (Keithley model 175A).

2.4. Procedures. (a) Assembly of PE-Coated Colloidal Particles onto Electrode Surfaces. PS nanospheres were first coated with several PE layers by utilizing the previously reported LBL self-assembly procedure.[51,52] PS particles coated with different PE layer numbers, denoted as PE_2−PS (two PE layers), PE_4−PS (four PE layers), and PE_6−PS (six PE layers), were diluted 400-fold. To assemble the PE-coated PS particles, a gold film or a QCM crystal was sandwiched between two Teflon

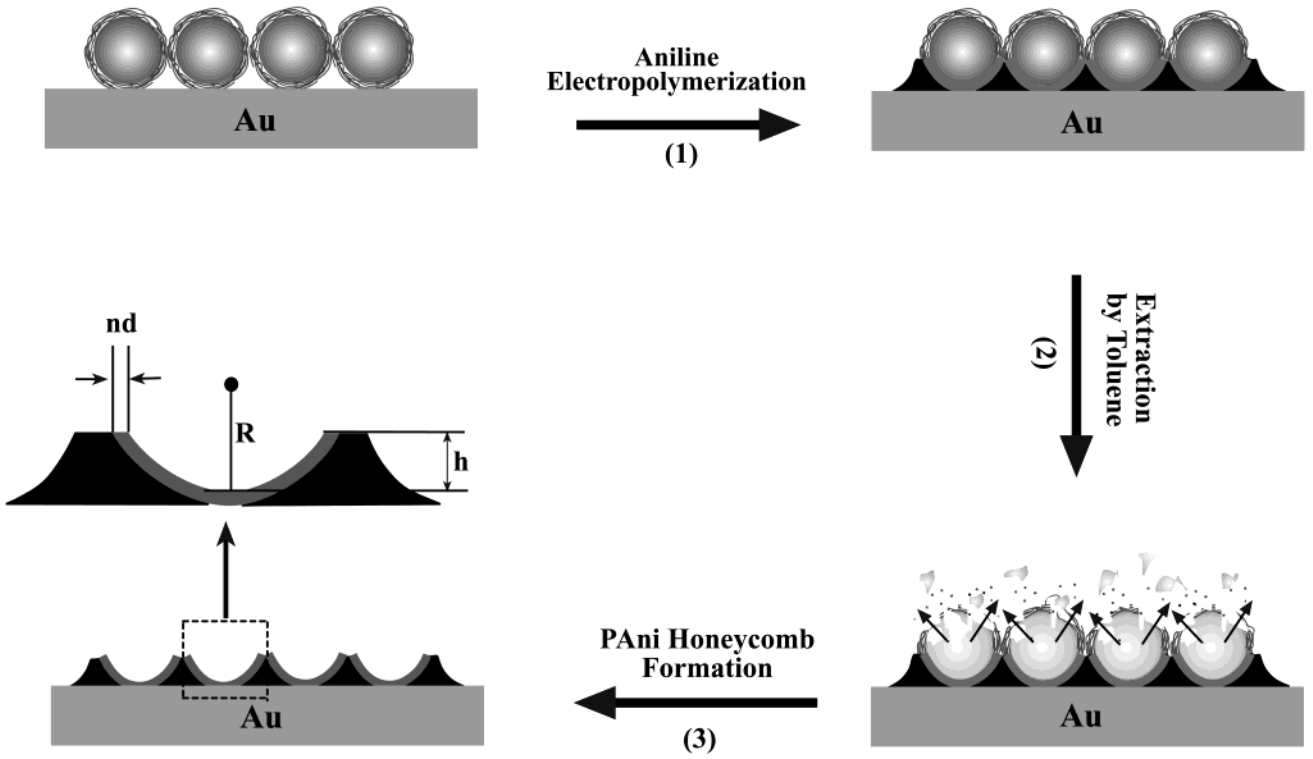

Figure 1. Schematic representation of the PAni honeycomb film fabrication. For clarity, the thin PE shells and the PS cores are not drawn to scale. The arrows in the core extraction step imply that the dissolution of the PS particles into the solution ruptures the PE caps that are in contact with the extraction solution. The parameters used for calculating the volumes of the interstitial voids and the PE shells are the radius of the PS particle (R), the depth of the honeycomb pore (h), the number of PE layers (n), and the average thickness of each PE layer (d).

blocks. After adding 80 μL of the solution containing the PE-coated PS particles into the solution well of the top block, the solvent was allowed to evaporate over a period of at least 2 days.

(b) Lithographic Patterning of Surfaces with PE-Coated Colloidal Particles and PAni Honeycomb Formation. A gold film or a QCM crystal covered with the PE-coated PS colloidal particles was immersed in a solution containing 0.5 M $HClO_4$ and 0.2 M aniline. Three consecutive potential cycles between −0.1 and 0.8 V versus a Ag/AgCl reference electrode were implemented to grow PAni films at the PE-coated PS particle (PE_n−PS) assemblies. After the electropolymerization, the PS cores were removed by placing the substrate in toluene for 24 h.

3. Results and Discussion

3.1. Fabrication of PAni Honeycomb Films. Figure 1 schematically depicts the procedure involving the electropolymerization of PAni within the interstitial voids among a preformed PE-coated colloidal particle assembly (step 1), the extraction of the PS particles using toluene (step 2), and the formation of the 2-D array of PAni honeycomb film with pores containing PE layers (step 3). Our previous work has shown that PS nanospheres coated with PDADMAC/PSS bilayers can self-assemble into 2-D hexagonally close-packed arrays[52] (a cutoff view is shown in this Figure). We and other researchers have demonstrated that small charged species can infiltrate the PE shells via electrostatic interaction.[51−53] In this work, the outermost PE shell (i.e, negatively charged PSS) serves as a surface that attracts the positively charged anilinium ions in the solution because a flow injection quartz crystal microbalance (FIQCM) measurement showed that anilinium ions were not affixed inside the PE shell for a prolonged period.[54] Thus, it appears that the aniline electropolymerization probably occurs first at a substrate surface in the interstitial voids and propagates to the aniline−monomer-covered PE shells. As delineated below, the volume occupied by the PE shell is almost negligible when compared to that of the interstitial voids. Hence, the major increase in the PAni deposition at the PE_n−PS assembly (vide infra) is not due to the film growth within the PE layer but to the uniformity of the PAni film at the PE_n−PS particles whose surfaces are parts of the interstitial voids.

Following the PS core extraction, a PAni honeycomb film can be produced. Note that the dissolution of the PS cores is shown in the schematic to rupture parts of the PE thin shells that were not covered with the PAni deposit. Formation of such a broken egg-shell PE structure upon core extraction has been reported in several studies.[8,52]

Figure 2a and b are AFM images of a PE_2−PS assembly and the changes to this assembly brought about by the PS core extraction, respectively. Clearly, a well-ordered PAni honeycomb film was formed. For comparison, thin PAni honeycomb films produced in the same fashion using a PE_4−PS assembly (Figure 2c) and an assembly containing bare PS particles (Figure 2d) are both presented. In producing these honeycomb films, the electrode potential was scanned between −0.1 and 0.8 V for three consecutive cycles with the scan terminated at −0.1 V. We found that doubling the cycle number leads to a thicker PAni film. For the PE_2−PS assembly, a well-ordered 2-D PAni honeycomb film could still be produced. However, for the PE_4− and PE_6−PS assemblies, the PAni growth was extended beyond the interstitial voids to cover the PE_n−PS particles. The subsequent extraction of the PS cores did not result in a PAni honeycomb film with evenly distributed pores. We found that three potential cycles are optimal for forming well-ordered PAni films with the various PE_n−PS assemblies employed in this study, making the comparison of the effect of PE layer numbers on the final honeycomb structures consistent.

TABLE 1: Geometric Parameters of PAni Honeycomb Films and Ratios between the Interstitial Void and PE Shell Volumes

	pore diameter (nm)	pore depth (nm)	wall width (nm)	density (pores/μm^2)	interstitial void volume per unit area (nm^3/nm^2)	PE shell volume per unit area (nm^3/nm^2)	volume ratio (%)[b]
bare	521 ± 69 (447[a])	100	153 ± 71 (243)[a]	2.49	73.0	0	
PE_2−PS	505 ± 23	110	162 ± 33	2.41	82.7	2.14	2.6
PE_4−PS	459 ± 26	110	210 ± 41	2.41	87.5	4.24	4.8
PE_6−PS	462 ± 97	112	206 ± 189	1.95	93.3	6.35	6.8

[a] Theoretical value corresponding to a 100-nm-deep pore. [b] The ratio of the interstitial void volume over the PE shell volume for a given film.

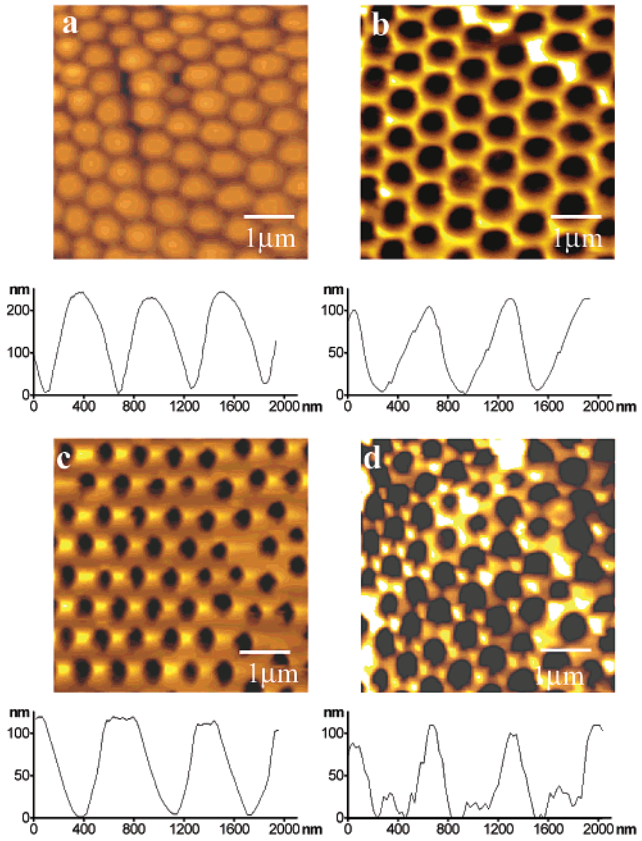

Figure 2. Topographic AFM images of (a) a gold surface covered with a close-packed PE_2−PS particle assembly, (b) a PAni honeycomb film generated by electropolymerization of aniline in the interstitial voids of (a) following core extraction, (c) a PAni honeycomb film produced using a PE_4−PS assembly, and (d) a PAni honeycomb film templated with a bare PS particle assembly. Representative cross-sectional contours are also presented to show the regularity of the patterns.

Figure 2a shows that the presence of the PE layers does not hamper the organization of a 2-D close-packed particle array. Such an observation has also been noted in our recent work.[52] It is also apparent from Figure 2b and c that such a periodic particle array was not disrupted by the PAni electropolymerization and the follow-up PS core extraction. The main differences between parts b and c of Figure 2 are the pore diameters and widths of the PAni walls. It is interesting that the use of a bare PS particle assembly did not produce PAni arrays as well-ordered as those templated with PE_n−PS particle assemblies (Figure 2d).

We also obtained SEM images of the various patterned surfaces in an attempt to assess the effect of the PE layers on the pore uniformity. PAni honeycomb structures formed with PE_2− and PE_4−PS assemblies (images not shown) are essentially identical to those shown in Figure 2b and c. The utilization of six alternating PDADMAC/PSS layers, however,

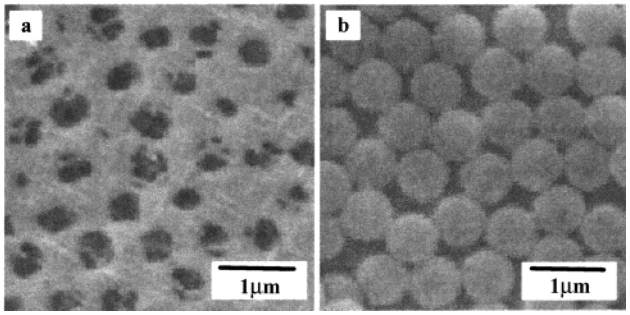

Figure 3. Scanning electron micrographs of (a) a PAni honeycomb film fabricated with the template of a PE_6−PS assembly and (b) an assembly of PE_6−PS particles.

introduced irregularity into the final structure (Figure 3a). The relatively nonuniform pore distribution can be attributed to the greater uncontrollability in packing the PS particles coated with a thicker PE multilayer. This is evidenced by the defects in the PE_6−PS assembly prior to the core extraction (Figure 3b). Another consequence of a thicker PE coating is its greater impediment to the core extraction. This point is reflected by the observation that the core extraction did not completely remove the PE shells. Some residual PEs from the ruptured PE shells can be found to cover parts of the PS particles in Figure 3a.

Table 1 lists the average diameter, depth, and density of the pores as well as the wall widths of the various PAni honeycomb films that were measured by AFM. The theoretical pore diameters and wall widths are functions of the pore depth (h). The sum of the interstitial and PE shell volumes (V) can also be calculated using the equation

$$V = \frac{1}{2\sqrt{3}(R+nd)^2}\left[2\sqrt{3}(R+nd)^2(h+nd) - \pi h^2\left(R-\frac{h}{3}\right)\right] \quad (1)$$

where R is the radius of the PS particle, n is the number of PE layers, and d is the average thickness of each PE layer (about 2 nm[55]). Because d is very small, the volume occupied by the PE layers is negligible for a finite n value when compared to V. Ratios between these two values are also provided in Table 1 for different n values.

Two points are worth noting upon evaluating the V value and the pore diameter. First, from the pore depth and the cross-sectional contours presented under the images in Figure 2, our predetermined electropolymerization parameters led to the deposition of films of an essentially constant thickness, which illustrates that the PE-coated nanosphere lithography provides a controllable route for making PAni honeycomb film of a desirable thickness. Second, the pore size changes in the order of bare PS > PE_2−PS > PE_4−PS ≈ PE_6−PS, whereas the density of the pores remains essentially unchanged. The only exception is given by the surface generated from the PE_6−PS

particle assembly. But this exception is contingent on the aforementioned difficulty in forming well-ordered arrays of colloidal particles coated with a large number of PE layers.

A plausible interpretation for the pore size variation might be a combination of the following two effects: (1) as the PE layer number increases, the adhesion of PAni becomes firmer and more uniform; consequently, the interstitial voids can be filled more compactly and (2) upon core extraction, the PAni honeycomb may shrink, but the extent of shrinkage decreases with the PE layer number. The first contention is supported by the increase in the PAni loading with the PE layer number, which was measured by EQCM during PAni growth (discussed below). Armes and co-workers showed that the maximum PAni coverage on PS particles in a colloidal solution was 57−59%, and they observed rather patchy PAni films at unmodified PS particles.[40] This effect is also manifested by the irregularity of PAni film produced from electropolymerization using the assembly of bare PS particles as the template (Figure 2d). Therefore, precoating PS particles with PE layers improves the uniformity of the PAni attachment to the colloidal surfaces and increases the amount of PAni that can be deposited in the interstitial voids (vide infra). As for the second contention, the shrinkage of PE layers[51,52] and the conduction of polymer films[7−9,24] upon exposure to organic solvents have been noted in some recent papers. It appears that the greater the PE number, the more rigid the PAni/PE composite shells around the pores. To gauge the extent of shrinkage and to understand the role of the PE layers, it is helpful to compare the theoretical pore diameter (447 nm for a 100-nm-deep pore) to the experimentally measured values. As shown in Table 1, the pore diameter becomes quite comparable to the theoretical value when $n \geq 4$. The percentages of PAni film shrinkage with respect to the theoretical value for the various films were estimated to be 37 (PAni produced with bare PS particles), 33 (PAni produced with PE_2−PS), 13 (PAni produced with PE_4−PS), and 15 (PAni produced with PE_6−PS). To afford the desirable pore periodicity and to strengthen the pore structures, we conclude that four alternating PE layers appear to be optimal.

3.2. EQCM Measurements. We conducted EQCM measurements of the amount of PAni deposited at surfaces covered with PE_n−PS assemblies. Shown in Figure 4 are representative cyclic voltammograms (CVs) and their corresponding mass−potential diagrams. Again, three cycles were implemented, and the potential scan was stopped at −0.1 V. The QCM responses indicate a continuous growth of the PAni film at surfaces modified with PE_n−PS assemblies. For the QCM response displayed in Figure 4b, a cumulative deposition of 49 ng was determined. The QCM results should be more reliable than those determined voltammetrically because the uncertainties associated with the charging current and the electrolytic efficiency (typically less than 100% for the electrosynthesis of conductive polymers) are not encountered.[30,31,49] The relationship between the amount of PAni deposited and the PE layer number revealed by the results in Table 2 suggests that the amount of PAni deposited increases with the PE layer number, a trend that is consistent with the AFM observation.

From a quantitative viewpoint, we can compare the PAni loading determined by EQCM to that predicted by the free volume available for PAni deposition (V). Although the volume defined by eq 1 contains both the interstitial spaces and the PE layers, it is worth reiterating that the inclusion of the PE layer as a medium for PAni deposition is not essential because of the small ratios of the PE shell volumes over the corresponding interstitial void volumes (Table 1).

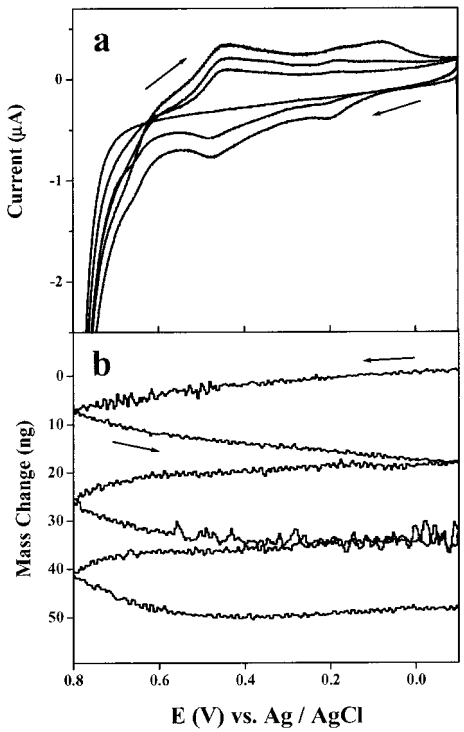

Figure 4. (a) Cyclic voltammograms of a PAni honeycomb film templated with a PE_2−PS assembly and (b) the mass−potential diagrams simultaneously acquired during three consecutive potential cycles. The electrolyte solution was 0.5 M $HClO_4$, and the scan rate was 0.05 V/s. Arrows indicate the scan directions.

TABLE 2: Mass Densities and Conductivities of PAni Honeycomb Films Formed with Different PE_n−PS Assemblies

	mass density (theoretical, $\mu g/cm^2$)	mass density (EQCM, $\mu g/cm^2$)	conductivity ($S\ cm^{-1}$)
bare	11.0	6.1	2.63×10^{-2} (3.14×10^{-2})[a]
PE_2−PS	12.4	7.9	2.47×10^{-2}
PE_4−PS	13.1	10.4	2.65×10^{-2}
PE_6−PS	14.0	12.1	2.77×10^{-2}

[a] Conductivity of a regular thin PAni film.

Perhaps the most interesting point is that the mass density of PAni determined by EQCM (Table 2) begins to agree with the theoretical predication once the PE_4−PS particle assembly is employed. With four of fewer PE layers (i.e., no PE or PE_2), a relatively large discrepancy exists between the theoretical and experimental values. Thus, the deviation of the PAni deposition from the value predicted on the basis of the free volume available for PAni growth supports our earlier contention about an inhomogeneous and incompact attachment of PAni onto colloidal surfaces in the absence of a sufficient number of PE layers.

3.3. Characterization of the PAni Honeycomb Films. Besides the morphology and the surface features, other essential properties of the PAni honeycomb films (e.g., conductivity, redox states, the composite nature of the pores, and the ion mobility within the films) were investigated. The conductivities of the various PAni honeycomb films were found to be highly comparable to that of a planar PAni film as well as to that of a macroporous PAni film formed via templating with multilayers of bare PS nanospheres (Table 2).[24,40−42,56]

Redox states of the PAni honeycomb films were probed using reflectance FTIR. Spectrum a in Figure 5 was acquired from a PAni honeycomb film patterned with a PE_2−PS assembly. The

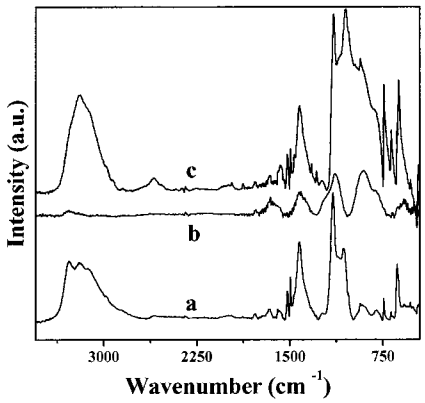

Figure 5. Representative reflectance FTIR spectra of (a) a PAni honeycomb film templated with a PE_2−PS particle assembly, (b) a 2-D array of thin PE shells composed of PDADMAC and PSS, and (c) a regular thin PAni film.

C−N bending (678 cm^{-1}) and the N−H stretching (3000−3200 cm^{-1}) in spectrum a are indicative of the existence of the leucoemeraldine moiety (structure shown on the left of the following reaction).[57] The peak at 1160 cm^{-1} corresponds to the leucoemeraldine C−N stretching, whereas peaks at 1500 and 1590 cm^{-1} are associated with the benzenoid and quinoid units, respectively.[8,57] The ratio of the area of the latter band to that of the former was found to be less than 1 (0.72), suggesting that the film is primarily benzenoid in nature.[57,58] This result is understandable because the potential scan for growing the PAni honeycomb film was terminated at a value (−0.1 V) where the reduced PAni form is prevalent. It is worth mentioning, however, that the presence of a C═N stretching band (1590 cm^{-1} [57]) indicates that the film may not have been completely reduced. Partial oxidation of the film by ambient air during spectral measurements may be responsible for the appearance of the C═N peaks.[59]

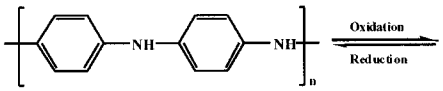

Benzenoid

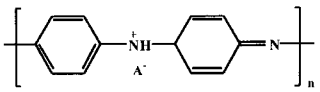

(2)

Quinonoid

To verify the composite nature of the inner walls of the pores, we compared the reflectance FTIR spectrum of a PAni honeycomb film produced using PE_2−PS (spectrum a), a film comprising only two PE thin layers (spectrum b), and a regular thin PAni film (spectrum c). Although the intensities of peaks associated with PAni predominate in the spectral regions where the PAni and PE peaks overlap, some peaks inherent to PE are still distinctive (e.g., the N−H stretching that is characteristic of the quaternary ammonium group on PDADMAC at 3280 cm^{-1} in spectrum b appears as a shoulder in spectrum a;[60,61] the peak associated with PSS at 915 cm^{-1} [62,63] is resolvable in spectrum a but absent in spectrum c). Therefore, despite the stronger intensity of the PAni peaks, the comparison of the FTIR spectra provided spectral evidence about the coexistence of PE and PAni in the honeycomb film.

Finally, we used EQCM to study the ion transport processes within the PAni honeycomb films. Parts a and b of Figure 6 are overlays of a series of steady-state CVs and the mass−potential diagrams simultaneously collected at different PAni honeycomb films. The voltammogram of a PAni honeycomb film is analogous to that of a regular PAni thin film in its shape and peak potential, implying that the redox properties of the PAni honeycomb structure are unperturbed by the presence of the small amount of PEs. The current from the PAni honeycomb structure is less intense than that from a regular PAni film because a large number of pores occupy the regions where PAni would be otherwise deposited. All of the films exhibited the mass−potential behavior that was expected from a regular PAni thin film. When the PAni films were oxidized from the leocuemeraldine (reduced) state to the emeraldine (oxidized) state at ca. 0.2 V, a large mass increase was observed. This mass increase can be attributed to the insertion of the perchlorate anion into the PAni film to maintain electroneutrality (refer to eq 2 that shows that an anion, A^-, has been incorporated into the film). When the emeraldine film was further oxidized to

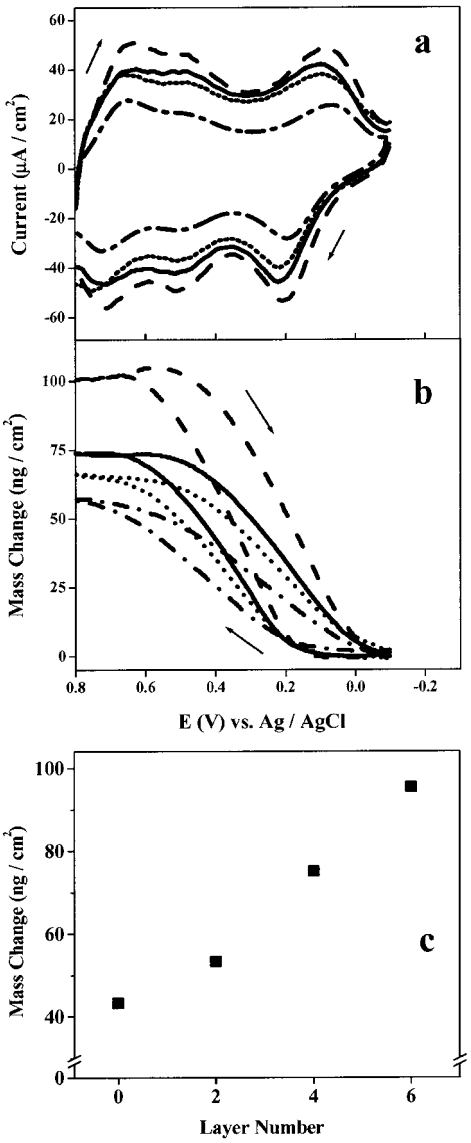

Figure 6. An overlay of (a) steady-state voltammograms and (b) the mass−potential diagrams of PAni honeycomb structures formed with assemblies of bare PS particles (−·−), PE_2−PS (···), PE_4−PS (− −), and PE_6−PS (− − −). All voltammograms were acquired from aniline-free 0.5 M $HClO_4$ solutions at a scan rate of 0.1 V/s. Arrows indicate the scan directions. Panel c shows the average steady-state mass changes of the various films plotted as a function of the PE layer numbers.

the permigraniline form at ca. 0.5 V, no appreciable mass change was observed. These observations are consistent with results from previous EQCM studies by Orata and Buttry[64] and Choi et al.[65] It was also found that the amount of anion incorporation increases with the number of PE layers (Figure 6c). Recalling that the quantity of PAni deposition changes in the order of $PE_6-PS \approx PE_4-PS > PE_2-PS >$ bare PS particles and realizing that the extent of anion incorporation should be proportional to the mass of the PAni film, we find that this trend is conceivable.

On the basis of the FTIR spectra, the conductivity measurements, and the EQCM findings, we conclude that the existence of the PE shells within the pores of the honeycomb structure does not affect the overall properties of the PAni honeycomb structure and that it even improves certain features of the PAni film (e.g., the mechanical robustness of the thin PAni walls is strengthened by the PE layers). Thus, PE-coated nanosphere lithography incorporating aniline electropolymerization provides a unique method for constructing well-ordered PAni honeycomb films with patterns that are tunable (the pore size and wall thickness can be varied by using different PE layer numbers and possibly by employing different-sized PS particles) and pores that are modifiable (different types of PEs can be utilized to change the charge polarity and density within the pores). We envision that charged species could be immobilized into the pores to develop useful sensors of large surface areas and that the well-ordered structures could be further exploited to fabricate devices of desirable patterns and functionalities.

Conclusions

Polyelectrolyte-coated nanosphere lithography involving aniline electropolymerization was developed to fabricate well-ordered 2-D polyaniline (PAni) honeycomb films. Through a systematic adjustment of the PE thickness and a judicious choice of the voltammetric parameters, the thickness of the PAni film can be controlled, and the dimensions of the pores (size, depth, and surface density) can be tailored. AFM and SEM were used to determine the morphology of the PAni film, the dimensions of the pores, and the extent of shrinkage of the PAni walls surrounding the pores. Reflectance FTIR and voltammetry were employed to examine the redox state of the resultant PAni honeycomb films, and the composite nature of the inner walls of the pores was verified through a comparison of the FTIR spectra of the honeycomb film and the PE layers. The amount of PAni deposited into the interstitial voids in the PE_n-PS assemblies was quantified by EQCM, and the results were compared to the values predicted by the volumes of the interstitial voids and the PE thin shells available for PAni deposition. The experimental and theoretical values became comparable when PE_4-PS nanospheres were assembled and served as the template. Packing the interstitial space with a larger quantity of PAni is attributable to the greater affinity of the anilinium ions toward the highly charged PE surface and the stability of the PAni deposit in the relatively hydrophobic environment within the PE layers. In the absence of the PE multilayers, patchy PAni films were attached to the PS nanospheres, and relatively irregular pores with varying diameters were observed upon core extraction. However, as the PE coating becomes thicker, more defects appear in the PE_n-PS assemblies. The optimal PE layer number for the maximum PAni deposition with a high regularity of the pattern is four. The PE shells were also found to enhance the rigidity of the PAni wall around the pores without altering other important properties of the PAni films (e.g., conductivity and conduit for ion transport within the films). PE-coated nanosphere lithography is a viable method for constructing well-ordered PAni honeycomb films with tunable and modifiable surface features. Such features or patterns might find important applications in sensor development and device fabrication.

Acknowledgment. Financial support from the NIH-SCORE subprojects (GM 08101), a NIH-AREA grant (GM 63530-01), and the donors of the Petroleum Research Fund administered by the American Chemical Society is gratefully acknowledged.

References and Notes

(1) Velev, O. D.; Lenhoff, A. M. *Curr. Opin. Colloid Interface Sci.* **2000**, *5*, 56−63.
(2) Johnson, S. A.; Ollivier, P. J.; Mallouk, T. E. *Science (Washington, D.C.)* **1999**, *283*, 963−965.
(3) Park, S. H.; Xia, Y. *Chem. Mater.* **1998**, *10*, 1745−1747.
(4) Weissman, J. M.; Sunkara, H. B.; Tse, A. S.; Asher, S. A. *Science (Washington, D.C.)* **1996**, *274*, 959−960.
(5) Jiang, P.; Bertone, J. F.; Colvin, V. L. *Science (Washington, D.C.)* **2001**, *291*, 453−457.
(6) Bertone, J. F.; Jiang, P.; Hwang, K. S.; Mittleman, D. M.; Colvin, V. L. *Phys. Rev. Lett.* **1999**, *83*, 300−303.
(7) Sumida, T.; Wada, Y.; Kitamura, T.; Yanagida, S. *Chem. Commun.* **2000**, 1613−1614.
(8) Wang, D.; Caruso, F. *Adv. Mater. (Weinheim, Ger.)* **2001**, *13*, 350−353.
(9) Cassagneau, T.; Caruso, F. *Adv. Mater. (Weinheim, Ger.)* **2002**, *14*, 34−38.
(10) Bartlett, P. N.; Birkin, P. R.; Ghanem, M. A. *Chem. Commun.* **2000**, 1671−1672.
(11) Deutsch, M.; Vlasov, Y. A.; Norris, D. J. *Adv. Mater. (Weinheim, Ger.)* **2000**, *12*, 1176−1180.
(12) Martin, C. R. *Acc. Chem. Res.* **1995**, *28*, 61.
(13) Macdiarmid, A. G.; Avlyanov, J. K.; Huang, F.; Huang, Z. Y.; Wang, H. L.; Wang, P. C.; Epstein, A. J. *Macromol. Symp.* **1997**, *118*, 445−450.
(14) Macdiarmid, A. G. *Synth. Met.* **1997**, *84*, 27−34.
(15) Velev, O. D.; Kaler, E. W. *Adv. Mater. (Weinheim, Ger.)* **2000**, *12*, 531−534.
(16) Davis, S. A.; Breulmann, M.; Rhodes, K. H.; Zhang, B.; Mann, S. *Chem. Mater.* **2001**, *13*, 3218−3226.
(17) Xia, Y.; Gates, B.; Yin, Y.; Lu, Y. *Adv. Mater. (Weinheim, Ger.)* **2000**, *12*, 693−713.
(18) Henze, H. P.; Antonietti, M. *Curr. Opin. Colloid Interface Sci.* **2001**, *5*, 343−353.
(19) Stein, A. *Microporous Mesoporous Mater.* **2001**, *44*−*45*, 227−239.
(20) Cho, G.; Glatzhofer, D. T.; Fung, B. M.; Yuan, W.-L.; O'Rear, E. A. *Langmuir* **2000**, *16*, 4224−4429.
(21) Cho, G.; Fung, B. M.; Glatzhofer, D. T.; Lee, J.-S.; Shul, Y.-C. *Langmuir* **2001**, *17*, 456−461.
(22) Sapp, S. A.; Mitchell, D. T.; Martin, C. R. *Chem. Mater.* **1999**, *11*, 1183−1185.
(23) Cepak, V. M.; Martin, C. R. *Chem. Mater.* **1999**, *11*, 1363.
(24) Bartlett, P. N.; Birkin, P. R.; Ghanem, M. A.; Toh, C. S. *J. Mater. Chem.* **2001**, *11*, 849−853.
(25) Velev, R. D.; Lenhoff, A. M.; Kaler, E. W. *Science (Washington, D.C.)* **2000**, *287*, 2240−2244.
(26) MaCarthy, G. P.; Armes, S. P.; Greaves, S. J.; Watts, S. P. *Langmuir* **1997**, *13*, 3686−3692.
(27) Lascelles, S. F.; Armes, S. P. *Adv. Mater. (Weinheim, Ger.)* **1995**, *7*, 864.
(28) Cairns, D. B.; Armes, S. P.; Bremer, L. G. B. *Langmuir* **1999**, *15*, 8025.
(29) Bard, A. J.; Faulkner, L. R. *Electrochemical Methods: Fundamentals and Applications*; Wiley & Sons: New York, 2001.
(30) Buttry, D. A. *Applications of the Quartz Crystal Microbalance to Electrochemistry*; Bard, A. J., Ed.; Marcel Dekker: New York, 1991; Vol. 17.
(31) Buttry, D. A.; Ward, M. D. *Chem. Rev.* **1992**, *92*, 1355−1379.
(32) Malinsky, M. D.; Kelly, K. L.; Schatz, G. C.; Van Duyne, R. P. *J. Phys. Chem. B* **2001**, *105*, 2343−2350.
(33) Jensen, T. R.; Malinsky, M. D.; Haynes, C. L.; Van Duyne, R. P. *J. Phys. Chem. B* **2000**, *104*, 10549−10556.
(34) Jensen, T. R.; Schatz, G. C.; Van Duyne, R. P. *J. Phys. Chem. B* **1999**, *103*, 2394−2401.
(35) Hulteen, J. C.; Treichel, D. A.; Smith, M. T.; Duval, M. L.; Jensen, T. R.; Van Duyne, R. P. *J. Phys. Chem. B* **1999**, *103*, 3854−3863.

(36) Hulteen, J. C.; Van Duyne, R. P. *J. Vac. Sci. Technol., A* **1995**, *13*, 1553−1558.
(37) Haynes, C. L.; Van Duyne, R. P. *J. Phys. Chem. B* **2001**, *105*, 5599−5611.
(38) Rossi, R. C.; Tan, M. X.; Lewis, N. S. *Appl. Phys. Lett.* **2000**, *77*, 2698−2700.
(39) Haynes, C. L.; McFarland, A. D.; Smith, M. T.; Hulteen, J. C.; Van Duyne, R. P. *J. Phys. Chem. B* **2002**, *106*, 1898−1902.
(40) Barthet, C.; Armes, S. P.; Chehimi, M. M.; Bilem, C.; Omastova, M. *Langmuir* **1998**, *14*, 5032−5038.
(41) Stejskal, J.; Kratochvil, P.; Armes, S. P.; Lascelles, S. F.; Riede, A.; Helmstedt, M.; Prokes, J.; Krivka, I. *Macromolecules* **1996**, *29*, 6814−6819.
(42) Stejskal, J.; Spirkova, M.; Riede, A.; Helmstedt, M.; Mokreva, P.; Prokes, J. *Polymer* **1999**, *40*, 2487−2492.
(43) Goren, M.; Lennox, R. B. *Nano Lett.* **2001**, *1*, 735−738.
(44) Fou, A. C.; Rubner, M. F. *Macromolecules* **1995**, *28*, 7115.
(45) Huang, Z.; Wamg, P. C.; MacDiarmid, A. G.; Xia, Y.; Whitesides, G. *Langmuir* **1997**, *13*, 6480.
(46) Decher, G. *Science (Washington, D.C.)* **1997**, *277*, 1232−1237.
(47) Tedeschi, C.; Mohwald, H.; Kirstein, S. *J. Am. Chem. Soc.* **2001**, *123*, 954−960.
(48) Briseno, A. L.; Song, F.; Baca, A. J.; Zhou, F. *J. Electroanal. Chem.* **2001**, *513*, 16−24.
(49) Briseno, A. L.; Baca, A.; Zhou, Q.; Lai, R.; Zhou, F. *Anal. Chim. Acta* **2001**, *447*, 123−134.
(50) Huang, E.; Satiapipat, M.; Han, S.; Zhou, F. *Langmuir* **2001**, *17*, 1225−1224.
(51) Wang, D.; Caruso, R. A.; Caruso, F. *Chem. Mater*. **2001**, *13*, 364−371.
(52) Han, S.; Shi, X.; Zhou, F. *Nano Lett.* **2002**, *2*, 97−100.
(53) Shi, X.; Cassagneau, T.; Caruso, F. *Langmuir* **2002**, *18*, 904−910.
(54) Shi, X.; Sanedrin, R. J.; Briseno, A. L.; Zhou, F. *Macromolecules*, submitted for publication.
(55) Sukhorukov, G. B.; Mohwald, H.; Decher, G.; Lvov, Y. M. *Thin Solid Films* **1996**, *284−285*, 220−223.
(56) Barthet, C.; Armes, S. P.; Lascelles, S. F.; Luk, S. Y.; Stanley, H. M. E. *Langmuir* **1998**, *14*, 2032−2041.
(57) Hatchett, D. W.; Josowicz, M.; Janata, J. *J. Phys. Chem. B* **1999**, *103*, 10992−10998.
(58) Hatchett, D. W.; Josowicz, M.; Janata, J. *J. Electrochem. Soc.* **1999**, *146*, 4535.
(59) Habib, M. A.; Maheswari, S. P. *J. Electrochem. Soc.* **1989**, *136*, 1050−1053.
(60) Anderson, M. R.; Davis, R. M.; Taylor, C. D.; Parker, M.; Clark, S.; Marciu, D.; Miller, M. *Langmuir* **2001**, *17*, 8380−8385.
(61) Caruso, F.; Furlong, D. N.; Ariga, K.; Ichinose, I.; Kunitake, T. *Langmuir* **1998**, *14*, 4559−4565.
(62) Urban, M. W. *Vibrational Spectroscopy of Molecules and Macromolecules on Surfaces*; Wiley & Sons: New York, 1993.
(63) Harris, J. J.; Bruening, M. L. *Langmuir* **2000**, *16*, 2006−2013.
(64) Orata, D.; Buttry, D. A. *J. Am. Chem. Soc.* **1987**, *109*, 3574−3581.
(65) Choi, S. J.; Park, S. M. *J. Electrochem. Soc.* **2002**, *149*, E-26.